AGU ADVANCING EARTH AND SPACE SCIENCE

Geophysical Research Letters®

RESEARCH LETTER
10.1029/2022GL097714

Key Points:

- True 3D structure and spatiotemporal evolution of large contiguous heatwave over China are tracked by the 3D connected component labeling algorithm
- Contiguous heatwaves in China exhibit distinct characteristics and evolution patterns in different geographical locations and time periods
- Substantial increases are observed in the frequency, area, magnitude, duration, and moving distance of contiguous heatwaves since the 1960s

Correspondence to:
Z. Liu,
pliuzhen@gmail.com

Citation:
Luo, M., Lau, N.-C., Liu, Z., Wu, S., & Wang, X. (2022). An observational investigation of spatiotemporally contiguous heatwaves in China from a 3D perspective. *Geophysical Research Letters*, *49*, e2022GL097714. https://doi.org/10.1029/2022GL097714

Received 7 JAN 2022
Accepted 6 MAR 2022

Author Contributions:
Conceptualization: Ming Luo
Formal analysis: Zhen Liu, Sijia Wu, Xiaoyu Wang
Funding acquisition: Ming Luo
Investigation: Ming Luo, Ngar-Cheung Lau, Zhen Liu, Sijia Wu, Xiaoyu Wang
Methodology: Ming Luo
Supervision: Ming Luo
Writing – original draft: Ming Luo
Writing – review & editing: Ngar-Cheung Lau, Zhen Liu, Sijia Wu, Xiaoyu Wang

An Observational Investigation of Spatiotemporally Contiguous Heatwaves in China From a 3D Perspective

Ming Luo[1,2], Ngar-Cheung Lau[2,3,4], Zhen Liu[5,6], Sijia Wu[1], and Xiaoyu Wang[1]

[1]Guangdong Key Laboratory for Urbanization and Geo-simulation | School of Geography and Planning | Guangdong Provincial Engineering Research Center for Public Security and Disasters, Sun Yat-sen University, Guangzhou, China, [2]Institute of Environment, Energy and Sustainability, The Chinese University of Hong Kong, Hong Kong SAR, China, [3]Department of Geography and Resource Management, The Chinese University of Hong Kong, Hong Kong SAR, China, [4]Program in Atmospheric and Oceanic Sciences, Princeton University, NJ, Princeton, NJ, USA, [5]Center for Climate Physics, Institute for Basic Science, Busan, Republic of Korea, [6]Pusan National University, Busan, Republic of Korea

Abstract Understanding the evolution of heatwaves is important for their prediction, mitigation, and adaptation. While most studies focused on either their temporal variability at individual station (or grid point) or the spatial variation over fixed durations, their daily joint evolution over space and time remains largely unexplored. Here, we investigate multi-dimensional characteristics of spatiotemporally contiguous heatwaves across China during 1961–2018 using observational data from a 3D perspective (i.e., latitude × longitude × time). Results obtained by the 3D identification show that large contiguous heatwaves in China exhibit distinct characteristics in different geographical locations and time periods. Heatwaves in northern areas prefer to move from west to east at a faster speed, persist longer, and have greater extent and intensity than southern heatwaves, which are generally originated from the east and move westward. It is also found that contiguous heatwaves are growing in frequency, magnitude, areal extent, duration, and traveling distance across China.

Plain Language Summary Known as episodes with temperature exceeding a certain threshold, heatwaves exert severe detrimental impacts on human health. Understanding their joint evolution at both temporal and spatial dimensions is beneficial for us to mitigate the adverse effects and adapt ourselves to future heatwave increases under global warming. However, previous studies mainly focused on either the temporal or spatial changes of heatwaves rather than their co-variability over both time and space. Here we introduce a new method, the 3D connected component algorithm, to track the 3D evolution of spatiotemporally contiguous heatwaves over China during 1961–2018 using observational data. We find that contiguous heatwaves over northern China prefer to move eastward at a faster speed, persist longer, and have greater extent and intensity than southern heatwaves, which are generally originated from the east and move westward. Contiguous heatwaves show significant increases in frequency, magnitude, coverage, duration, and traveling distance.

1. Introduction

Heatwaves have set new temperature records over most of the world recently, posing severe threats to humans and the ecosystems (García-León et al., 2021; Perkins-Kirkpatrick & Lewis, 2020). For example, western Europe and Scandinavia experienced record-breaking temperatures in the summer of 2019, leading to almost 400 deaths in the Netherlands and 1,500 deaths in France (Watts et al., 2021). In China, heat-related mortality reached 26,800 deaths in 2019, which has risen from 1990 by four times (Cai et al., 2021). Moreover, heatwaves are projected to intensify in terms of frequency, intensity, and duration under future global warming and local human activities such as urbanization (Luo & Lau, 2021; Wang et al., 2021).

Heatwaves are often defined as episodes of three or more successive days with near-surface air temperatures exceeding a certain threshold, that is, the 95th percentile of daily temperatures over the reference period (Perkins & Alexander, 2013; You et al., 2017). Based on this definition, many studies have focused on heatwave investigation about its temporal (e.g., frequency and duration) and spatial (e.g., areal extent) characteristics. For example, previous researches tracked heatwaves temporally at station or grid point level and examined the variabilities or long-term changes in the frequency, intensity, and duration of heatwaves at stations or grid cells (Luo & Lau, 2017; Perkins-Kirkpatrick & Lewis, 2020). Also, some studies examined the spatial extent of heatwaves by

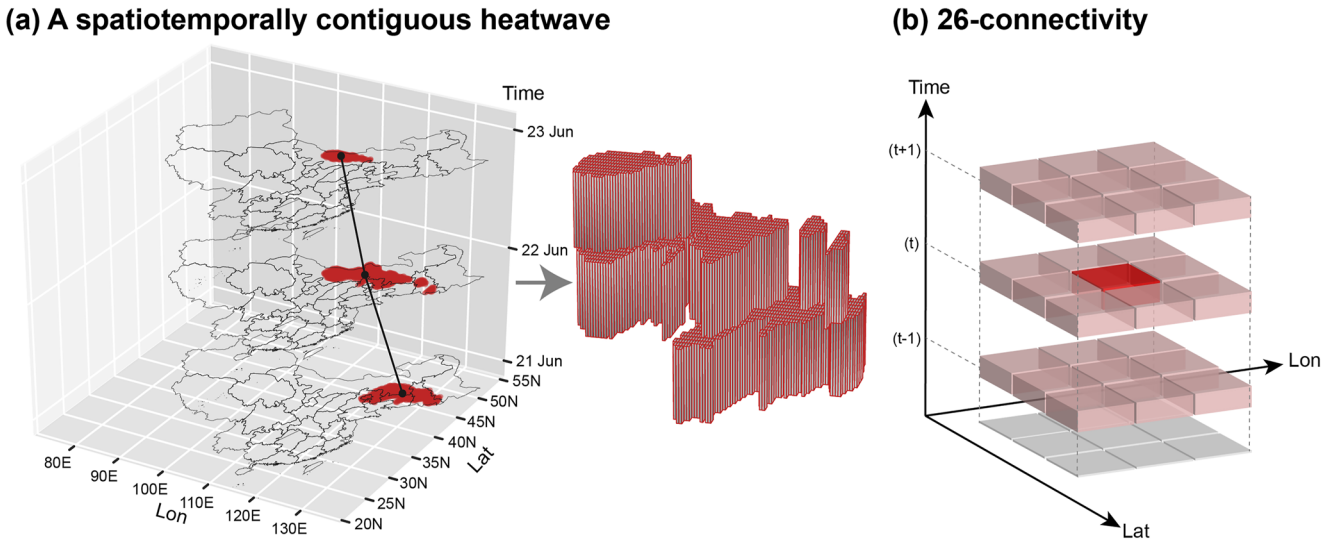

Figure 1. (a) The 3D evolution of a spatiotemporally contiguous heatwave event during 21–23 June 1961 in China; (b) the 26-connected 3D structure for tracking spatiotemporally contiguous heatwave event along the dimensions of latitude, longitude, and time (i.e., $t-1$, t, $t+1$). In (a), black dots indicate the intensity-weighted centroid across all days of the event. In (b), the 26 voxels connected with the center red voxel are marked by pink color, and the gray shading represents the projection of the 3D structure onto the latitude × longitude surface.

considering the proportion of grid cells that experienced a hot day or heatwave event (Lyon et al., 2019; Mukherjee & Mishra, 2021; Sharma & Mujumdar, 2017). For instance, Lyon et al. (2019) investigated the areal extent of spatially contiguous heatwaves in the United States and suggested the increasing extent of such events under the RCP8.5 scenario. However, these studies mainly analyzed the heatwave behaviors from either their temporal changes or spatial coverage separately, and neglected the spatiotemporally contiguous property of heatwaves.

Heatwaves often propagate across both space and time, thus exhibiting a spatiotemporal continuity. Here, we explore the co-variability of heatwaves over both time and space by tracking the life cycle of each heatwave. To distinguish from stagnated heatwaves over either time or space in previous studies, we name these heatwaves with 3D structures as contiguous heatwaves. This means that the spatial extent of contiguous heatwaves may vary over time during their lifespan (see an example in Figure 1a). It is thus important to track the evolution of heatwaves in both space and time simultaneously (i.e., 3-dimensional) by considering their spatiotemporal connectivity, which is, however, largely unexplored in previous studies. Only few studies have examined the characteristics of contiguous heatwaves, and these studies mostly focused on investigating the extremes in the United States (Keellings & Moradkhani, 2020; Lyon et al., 2019). For example, Keellings and Moradkhani (2020) tracked heatwaves in different subregions of the United States using geometric concepts and clustering algorithms and found an increased extent of contiguous heatwaves as well. Nevertheless, these studies concentrated on the frequency, duration, and areal extent; however, other properties (e.g., dynamic evolution properties including moving direction and traveling distance) of contiguous heatwaves remain much less understood. Particularly, spatiotemporally contiguous heatwaves in China have not been examined and hence require a thorough investigation.

In this study, we investigate the observed changes in spatiotemporally contiguous heatwaves over China during 1961–2018 by tracking their "true" 3D structures in both space and time. This investigation will provide an understanding of how multiple metrics of large contiguous heatwaves have changed in China since the 1960s. Our examinations from a 3D perspective can also provide an important reference for understanding the spatiotemporal dynamics of other types of extreme weather and climate events (e.g., extreme precipitation, flood, and drought).

2. Data and Methodology

2.1. Data

The main observational data is the daily gridded temperature data set of CN05.1, which covers the period of 1961–2018 (J. Wu & Gao, 2013). The gridded data set has been developed by interpolating 2,416 stations across

the mainland of China after strict quality control (J. Wu & Gao, 2013). We use the 0.25° × 0.25° grid resolution data for further analyses. The CN05.1 data set has been widely used in observational studies over China and in evaluating the performance of climate models (Dong et al., 2015; Ge et al., 2021; D. Li et al., 2018).

2.2. Spatiotemporally Contiguous Heatwaves

In this study, spatiotemporally contiguous heatwaves are tracked based on gridded daily maximum temperature (T_{max}) values using the 3-D connected component (CC3D) algorithm (Silversmith, 2021). The CC3D algorithm is an elaboration into 3D images of the 2D image connected components labeling (CCL) algorithm developed by Rosenfeld and Pfaltz (1966), and is implemented in the Python package *connected-components-3d* (https://pypi.org/project/connected-components-3d/). The CC3D method has been used to segment different cells or organs (e.g., kidneys and tumors) in medical studies (O'Reilly et al., 2021; Park et al., 2021; Zhao et al., 2020), and it also demonstrates potential in identifying connected events in climatological research (Reddy et al., 2021). The procedure of the method is briefly introduced as follows by starting with 2D CCL.

For a 2D "0/1" binary image, this CCL algorithm scans, and every time it first encounters a "1" foreground pixel (e.g., grid with extreme high temperature in our study), it marks the pixel with a new label. If there is a preexisting label in the neighborhood of this pixel, it uses that preexisting label instead. Whenever two labels are adjacent, the algorithm records that they are equivalent so that they can be relabeled consistently in the second pass. In the second pass, the pixels are relabeled using the equivalency table, which establishes one label as the root label of a tree and the root is considered as the representative label. Each pixel is then labeled with the representative label. The above procedures are well illustrated in a video at https://www.youtube.com/watch?v=ticZclUYy88. Similarly, the CCL algorithm can move to a 3D 26-connected neighborhood, and search for all 26-connected components in 3D images. To speed up the CCL algorithm, a two-stage strategy is also used (Silversmith, 2021; K. Wu et al., 2005). In the first stage, a decision tree is used to minimize the work performed in the scanning phase of the labeling algorithm, and in the second stage, a simplified union-find data structure is used to represent the equivalence information among the labels (K. Wu et al., 2005).

For each summer (i.e., June–August), we first convert the original T_{max} values that are stored in a 3-D array of voxels (i.e., with dimensions of latitude × longitude × time) into "0/1" binary format. Here, the "1" voxel indicates a hot day at the grid point that its T_{max} exceeds the corresponding 95th percentile threshold, while the "0" voxel says not. The 95th percentile on a calendar day is computed from the set of all daily T_{max} values over the 15-day window centering over the same calendar day during the reference period of 1961–1990 (i.e., a set of $15 \times 30 = 450$ days). Then, the "0/1" binary array is imported into the CC3D algorithm to search all possibly connected voxels (i.e., also known as super voxels) by setting the connectivity as 26 (Figure 1b). A 26-connected super voxel indicates a spatiotemporally contiguous heatwave event. The selection of 26 connectivity considers all adjacent grid points and neighboring days around the center grid cell in a $3 \times 3 \times 3$ cube, that is, $3 \times 3 = 9$ grids in the previous day, $3 \times 3 - 1 = 8$ grids excluding the center grid in the current day, and $3 \times 3 = 9$ grids on the following day (Figure 1b). It can track the contiguous heatwaves both in space and time jointly by allowing all 26-connected "1" voxels to be aggregated into a 3D structure that indicates an individual contiguous event. The 26-connectivity searching allows that a contiguous heatwave event occurring at a grid on the current day can move to the adjacent grids in the following day (see an example in Figure 1a), and ensures that different contiguous heatwave events are not overlapped or touched in the "latitude × longitude × time" space, that is, different events are neither spatially adjacent nor temporally contiguous.

Compared with the 3D identification, conventional methods based on fixed grid can only determine the life cycle of the heat events at fixed grid, and cannot track the events traveling from one place to another place. As an example, Figure 1a illustrates the 3D evolution of a spatiotemporally contiguous heatwave occurring during 21–23 June 1961. The life cycle of the heatwave is bounded by the first day and the last day of the 3D structure along the time dimension (i.e., the height of the 3D structure). This contiguous heatwave started as a small event on 21 June over Northeast China, and it grew larger and broke into several parts on the second day of its lifespan (i.e., 22 June). On 23 June, the event persisted with individual parts combined, continued to move westward, and covered central Inner Mongolia.

Table 1
Summary of the Metrics Used in This Study to Characterize Spatiotemporally Contiguous Heatwaves

Category	Metric	Description
Magnitude	Total magnitude (10^6 km^2 × °C)	Area-aggregated sum of the temperature exceedance relative to the threshold over all grid cells across all days of the event
	Intensity (°C)	Area-weighted average of the temperature exceedance over all grid cells across all days of the event
Area	Total area (10^6 km^2)	Sum of the areal extent of all grid cells across all days of the event
	Maximum area (10^6 km^2)	Projected area over longitude-latitude surface of the event, that is, the potentially maximum area affected by the event
Duration	Lifetime (days)	Time interval between the beginning and end of the event (i.e., the height of the 3D contiguous heatwave structure)
	Median duration (days)	Median value of the durations of all grid cells associated with the event
Evolution	Total moving distance (km)	Sum of the centroid moving distance between adjacent time steps over the whole lifespan of the event
	Moving speed (km/day)	Ratio of the total moving distance of the event to the lifetime of the even
	Moving direction	Directional angle from the centroid location of the first half of the event to the second centroid location of the event

2.3. Metrics of Spatiotemporally Contiguous Heatwaves

A spatiotemporal contiguous heatwave is represented by a 26-connected 3D structure in the space-time domain, and this 3D structure exhibits different properties. In our investigations, we focus on five different categories of metrics for characterizing the spatiotemporally contiguous heatwaves, that is, frequency, magnitude, areal extent, duration, and evolution (Table 1). The evolution pattern, as characterized by total moving distance, moving direction, and moving speed, is derived from the centroids of the 3D heatwave event. Here, the centroid of an event is calculated as the weighted average of the geographical coordinates (i.e., latitude and longitude) of all participating grid cells across all days of the event by weighting the temperature exceedance relative to the threshold (i.e., 95th percentile). The definitions of the metrics for 3D contiguous heatwaves are detailed in Table 1.

In this study, we focus on the largest and presumably most impactful heatwaves, and we select the events with a lifetime ≥3 days and maximum area ≥1 million km^2. This selection leaves 355 large contiguous heatwave events occurring in the mainland of China during 1961–2018 (Figure 2). The yearly statistics of the heatwave metrics during the study period are calculated by averaging all heatwave events occurring in the summer season of the corresponding year. The long-term trends in the yearly series of multiple heatwave metrics are estimated by the simple linear regression, with the significance evaluated by the modified non-parametric Mann-Kendall test at the 0.05 level of significance (Hamed & Rao, 1998).

3. Results and Discussion

3.1. Climatologies of Spatiotemporally Contiguous Heatwaves in China

We first provide the spatial distribution of the identified 355 large contiguous heatwaves across China during 1961–2018. Figure 2a shows a map of the geographical location of the event centroids of these contiguous events, with the corresponding total magnitude and intensity of contiguous heatwaves marked by the size and color of the circle, respectively. In summer, contiguous heatwaves occur nearly over the whole China. These events have an average affected area (i.e., the maximum projected area of the 3D heatwave event onto the latitude × longitude surface, see Table 1) of 2.59 million km^2 and intensity of 1.02°C in terms of temperature exceedance (Figures 2b and 2c), with an average temperature of 29.03°C. There is a noticeable tendency for the centroid of the largest heatwave events to cluster around Inner Mongolia (Figure 2a). This is an example of the "mid domain effect", which is partially caused by the limitation of the study area boundary (Colwell & Lees, 2000; Mondal & Mishra, 2021). Whilst beyond the scope of the current paper, it is also interesting to construct a geographically constrained examination, which requires complete data coverage across the study area. This is not possible with the CN05.1 data set, and a partial solution is to employ our methods to a spatially complete data set such as the

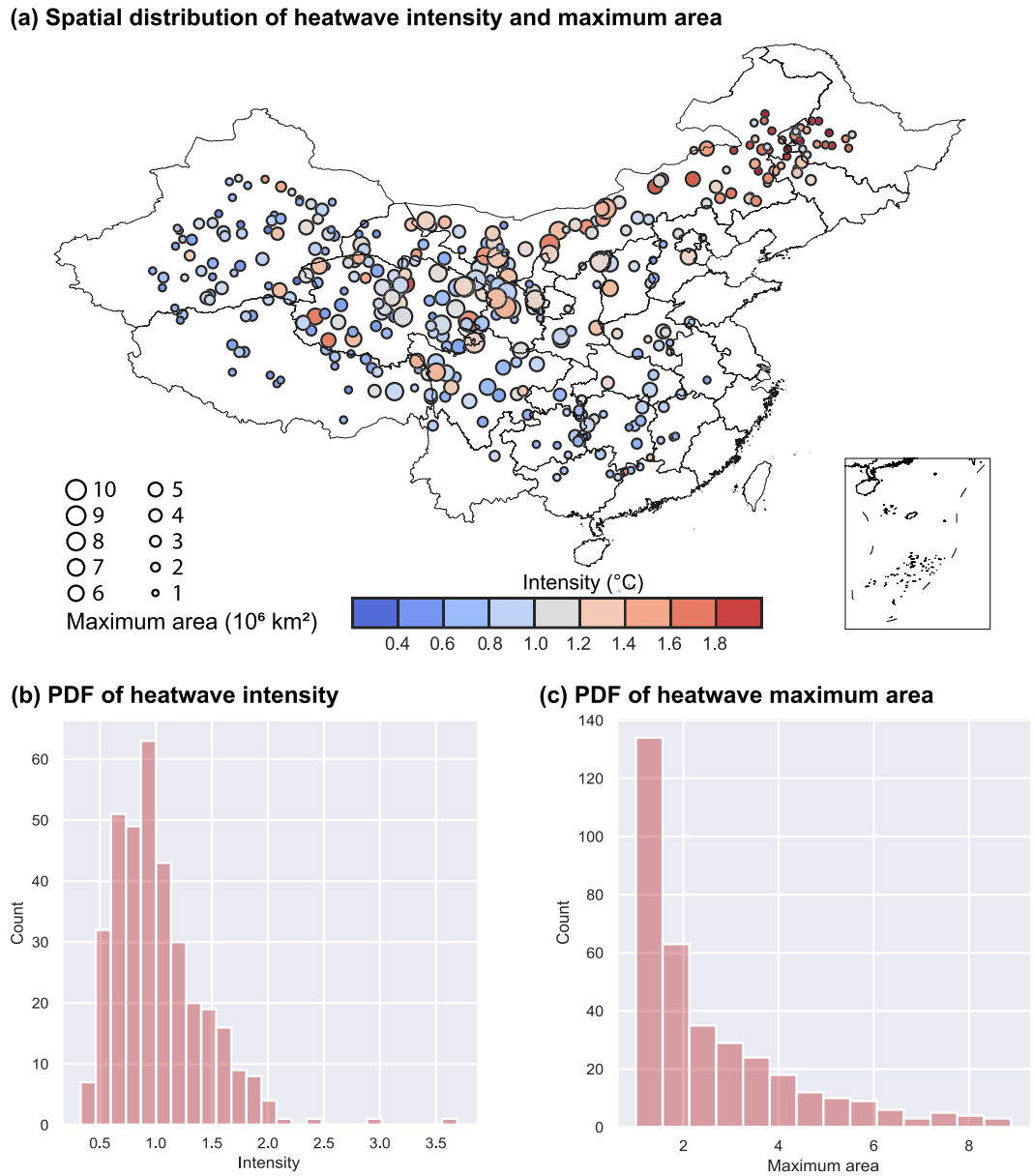

Figure 2. (a) Distribution of the overall centroids of contiguous heatwaves in China during 1961–2017, with the circle color and size representing the intensity and total magnitude, respectively; (b and c) Probability distribution functions (PDFs) of intensity and total magnitude of contiguous heatwaves.

ERA-5 reanalysis. As notably seen in Figure 2, heatwaves occurring in the southern China (i.e., south of 30°N) have smaller intensities and affected areas (i.e., on average by 0.23°C and 0.81×10^6 km^2, respectively) than those in northern China, which have an average intensity of 1.05°C and affected area of 2.70×10^6 km^2. The northern regions tend to show higher values of heatwave intensities, indicating possible amplification of high temperature extremes in these areas. The strongest intensity of the heatwaves occurs in northeast China and is larger than 1.8°C (Figure 2a), with a few events exceeding up to 3.5°C (see also Figure 2b). The heatwaves in southern and western China generally have intensities less than 1.0°C.

The spatiotemporal evolution of the contiguous heatwaves across China is mapped in Figure 3a. The tail of arrows indicates the location of the severity-weighted centroid of the first half of the contiguous heatwave event, while the head points to the centroid location of the second half of the event. A similar approach has been used to represent the evolution of drought events (Guo et al., 2018; Lloyd-Hughes, 2012). The rose diagrams in

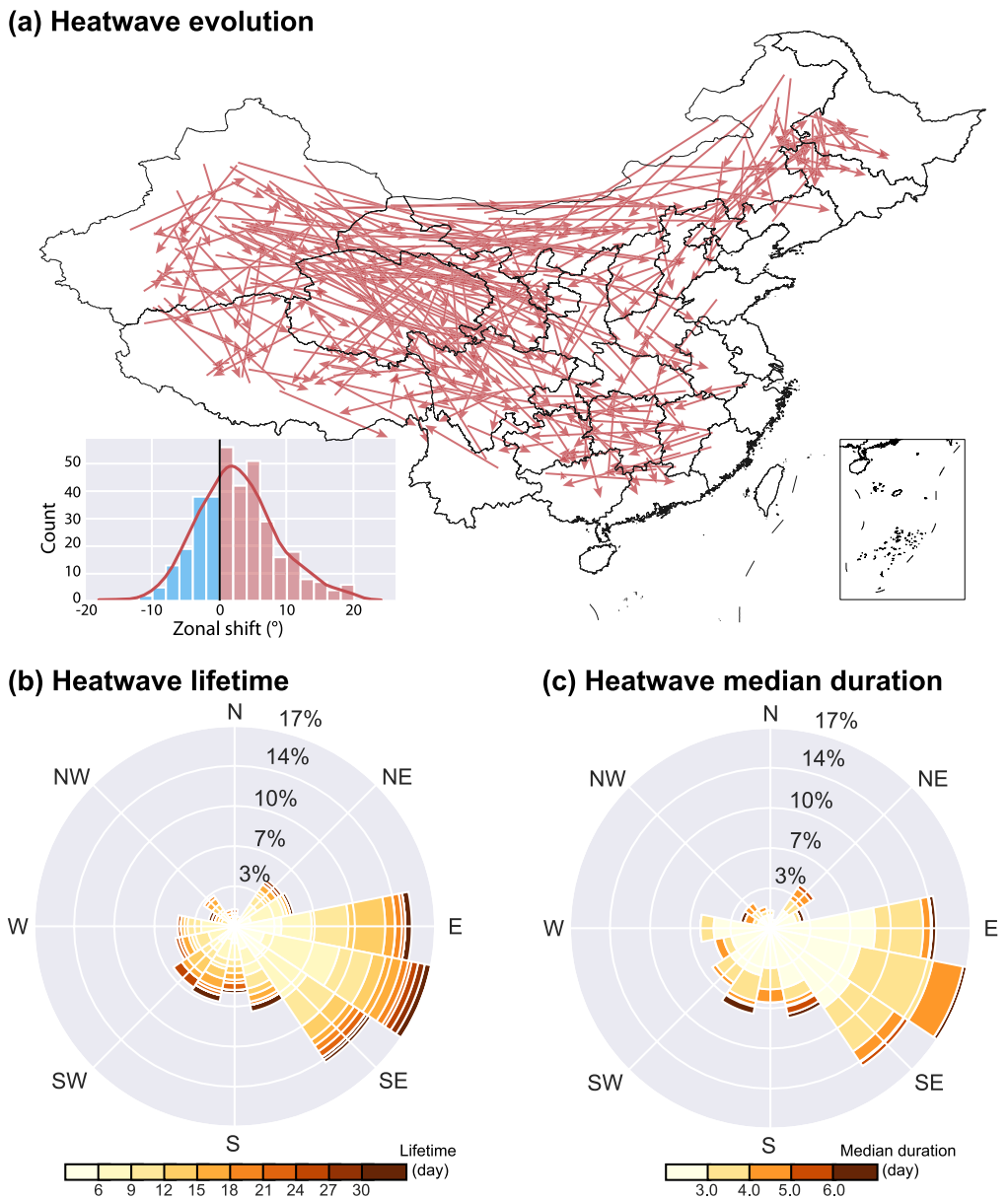

Figure 3. (a) Spatial and temporal evolution of contiguous heatwaves in China during 1961–2018, with the embedded chart showing the Probability distribution function of the zonal shift along the parallels; Rose diagram showing the distribution of moving direction associated with lifetime (b and c) and median duration (c) of contiguous heatwaves in China during 1961–2018. The tail (head) of each arrow in (a) indicates the centroid location of the first (second) half of the event. The rose diagram illustrates the directional distribution of the shifts in the event centroids.

Figures 3b and 3c are used to illustrate the directional distribution of heatwaves, with color indicating the lifetime (Figure 3b) and median duration (Figure 3c). The directions of heatwave propagation in Figure 3 indicate that heatwaves prefer to shift from west to east, particularly more prominent in western and northern regions of China, likely in relation to the effects of the East Asian subtropical westerlies over the mid-latitudes. Whereas, the southeastern parts tend to receive heatwaves originating from the east. This contrast is consistent with different sources of heat flow in different subregions of China, as noted in previous studies (Lu & Chen, 2016; Luo & Lau, 2017; Luo et al., 2020). It has been suggested that heatwaves in northwestern China are often accompanied by the westward movement of anomalously atmospheric blocking associated with the progression of Rossby waves in the upper-level troposphere (Luo et al., 2020; Pfahl & Wernli, 2012). The eastward propagation of the mid-latitude Rossby wave trains from the west (e.g., the North Atlantic) has also been suggested to contribute to

summer extreme precipitation events in the Eurasian continent (Ning et al., 2021; Saeed et al., 2014). In contrast, heatwaves in southeastern China are mainly triggered by the westward movement and extension of the western North Pacific subtropical high (WNPSH) (Ding et al., 2010; Luo & Lau, 2017).

The shift distance of the large contiguous heatwaves is indicated by the arrow length in Figure 3a. The average shift distance for all heatwaves over China is 598.1 km, with an average lifetime of 10.8 days. The increasing tendency of the shift distance with increasing latitude is prominent. Longer shift distances are mostly located in the northern regions, corresponding to eastward traveling heatwaves there, and the lower values of the shift distance can be observed in the southern regions (Figure 3a). These eastward-shifted heatwave events in northwest-north China also tend to persist for a longer period, in terms of longer lifetime and median duration (Figures 3b and 3c). The heatwaves that move eastward (mostly in western and northern regions) have an average lifetime of 11.63, which is slightly longer than those move westward (mostly in the south), that is, 10.47 days. On average, the contiguous heatwaves that move eastward have an average total moving distance of 1,454.6 km and travel at a speed of 191.5 km/day, which is slightly slower than the propagation speed of the Rossby wave (T. Li, 2006). Whereas, the events moving westward have a total moving distance of 1,025.4 km on average, at a mean speed of 142.5 km/day.

3.2. Long-Term Changes of Spatiotemporally Contiguous Heatwaves in China

We now proceed to investigate the long-term trends associated with different metrics of large contiguous heatwaves in China (Figure 4). The observed metrics for contiguous heatwaves across China show pronounced interannual variabilities. The heatwave metrics well capture the extreme heatwave years of 2010 and 2013, which are commonly known as extremely long-lived and highly impactful historical events in China (K. Chen et al., 2015; Gu et al., 2015; Wang et al., 2017). Figure 4 also shows that positive trends are observed in all metrics of the contiguous heatwaves. Extreme contiguous heatwaves in China have become more likely through the record (at the 0.05 significance level) in all dimensions of the heatwave risks including frequency, magnitude, intensity, area, duration, and traveling distance.

The frequency of large contiguous heatwaves in China demonstrates a nearly two-fold increase, at a rate of 0.539 events per decade (Figure 4a). The total magnitude and accumulated area of heatwaves also nearly doubled since the 1960s (Figures 4b and 4d), and this increase is mainly attributed to the substantial increase in the maximum area (Figure 4e) and durations (including both the lifetime and median duration) of the heatwaves (Figures 4f and 4g). The heatwave intensity, as measured by the temperature exceedance, also exhibits a significant increasing trend, that is, +0.042°C per decade (Figure 4c). With a prolonging heatwave lifetime, which has increased to longer than 2 weeks in most recent years, the total traveling distance of the contiguous heatwave events shows a rapid increase of +446.7 km per decade (Figure 4h). The moving speed of heatwaves does not show significant increasing or decreasing trends over the past decades (not shown).

The increasing regional trends in the frequency, magnitude, areal extent, and duration of 3D contiguous heatwaves are consistent with global warming and possible rapid regional/local urbanization in China (Luo & Lau, 2021; Ren & Zhou, 2014; Sun et al., 2016). The significant rises in multiple metrics of contiguous heatwaves as revealed in our study also echo the intensifying trends as reported in previous studies (Y. Chen & Li, 2017; Liao et al., 2018; Lu & Chen, 2016; You et al., 2017), except that most of these studies either examined the temporal variability of heatwaves in fixed reference area or focused their spatial heterogeneity over fixed durations.

4. Conclusions

Many previous studies suggested that heatwave events have increased in frequency, intensity, and duration over most of the world, including China. However, most of them regularly examined these temporal changes at station or grid point level and did not examine the spatiotemporal behaviors jointly and failed to consider the events as continuous in time and space. In this study, we track the spatiotemporally contiguous heatwaves across China by a 3D identification approach. We provide a new perspective of spatiotemporal connectivity of heatwaves to deepen the understanding of heatwave lifecycle in multiple dimensions. We also suggest multiple metrics to characterize various spatiotemporal properties of these contiguous heatwave events (see Table 1). These metrics are recommended for measuring other kinds of extreme weather and climate events (e.g., extreme precipitation and flood events).

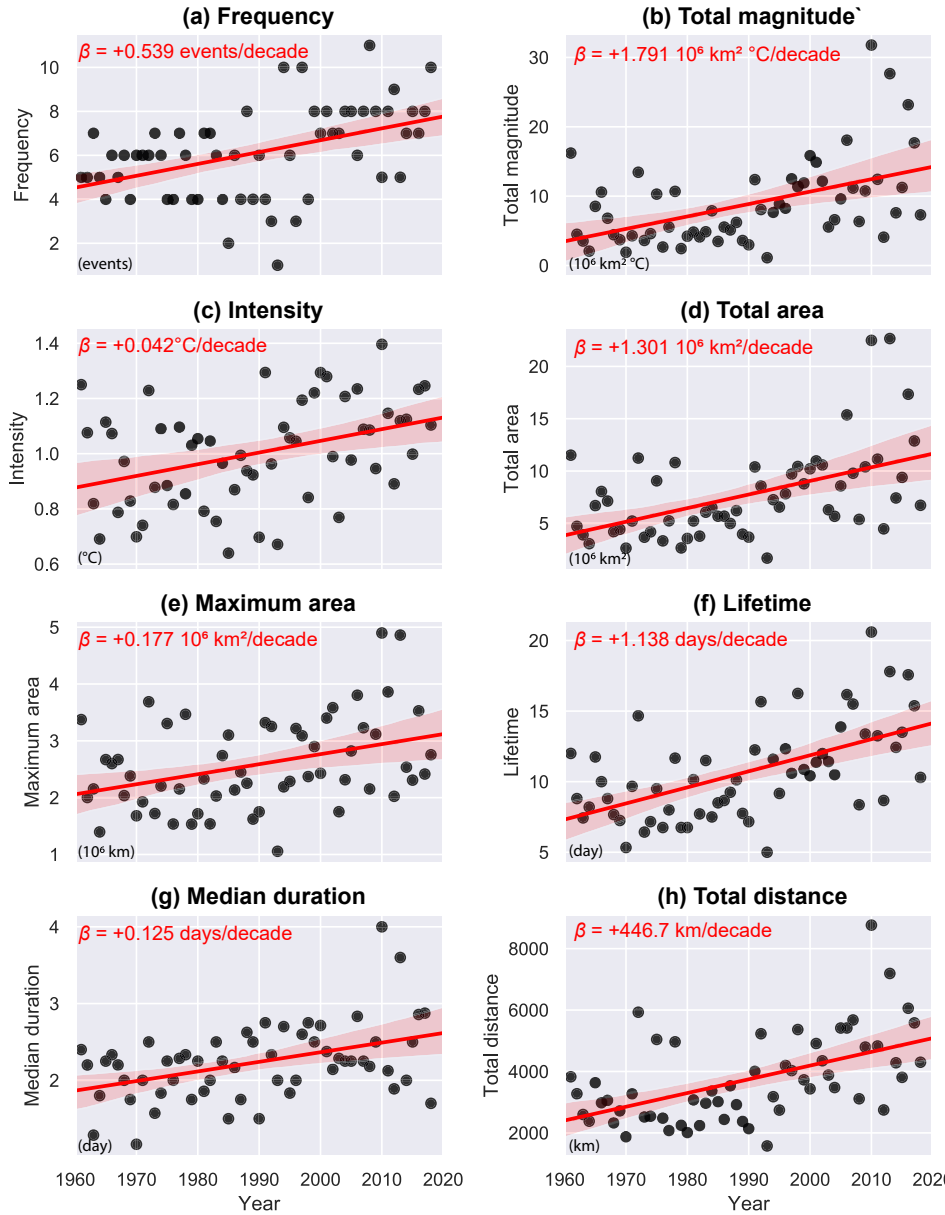

Figure 4. Observed temporal changes of multiple metrics of contiguous heatwaves in China during 1961–2018. The straight line indicates the corresponding linear trend, and all trends are statistically significant at the 0.05 level. The red shading indicates the 95% confidence interval of the fitted line.

Our results show that the 3D identification approach can capture the "true" 3D structure of spatiotemporally contiguous heatwaves well. This approach has been proven to be highly efficient and has a high performance in tracking spatiotemporally-connected 3D voxels. More importantly, it does not require any other parameter and is thus highly recommended in future similar studies. Applying this approach, 355 large contiguous heatwaves with affected area ≥1 million km^2 and lifetime ≥3 days are identified in the mainland of China during 1961–2018. The heatwave properties vary considerably across the space, and the properties of one individual event also vary greatly over time (e.g., varying spatial extent within its lifespan). Most of these contiguous events persisted for longer than 10 days and affected more than 2 million km^2.

The results obtained by tracking the true 3D structure of contiguous heatwaves reveal that contiguous heatwaves in the northern parts of China seem to have a larger areal extent and stronger magnitude than those in the south. The contiguous heatwaves in northwestern and northern China tend to move from west to east and travel longer

distances with higher moving speed, closely linked to the eastward propagation of the Rossby wave and atmospheric blocking. In contrast, the contiguous heatwave events in southern China generally develop from the east and move westward, in relation to the westward extension of the WNPSH. In addition, results by examining the long-term trends in multiple metrics of contiguous heatwaves show that spatiotemporally contiguous heatwaves are growing in terms of increased frequency, magnitude, areal extent, duration, and tracking distance across China since the 1960s.

Note that the spatiotemporally contiguous heatwaves examined here are defined by daily T_{max} values with broad applications in relevant climate change studies, and humidity is not considered in our study. Humidity is known to exacerbate thermal stress and increase the health-related impacts of heatwaves; thereby, contiguous heatwaves with combined effects of high temperature and high humidity are worth investigating. Also, our current investigation focuses on the historical changes of the large contiguous heatwaves during 1961–2018, and it is of great interest to extend such investigation to examine the future event changes under different socioeconomic scenarios. Besides, attribution of the secular trend in historical heatwave metrics to various drivers is beyond the scope of this paper and warrants further investigations in future work.

Data Availability Statement

The main observational data are the daily gridded temperature data set of CN05.1 (J. Wu & Gao, 2013), which is available at http://ccrc.iap.ac.cn/resource/detail?id=228.

Acknowledgments
This work is supported by the National Natural Science Foundation of China (41871029), the National Key R&D Program of China (2019YFC1510400), and the Science and Technology Program of Guangzhou (202102020489). Dr. Ming Luo is supported by the Pearl River Talent Recruitment Program of Guangdong Province (2017GC010634). Dr. Zhen Liu is supported by the Institute for Basic Science, Republic of Korea (IBS-R028-D1).

References

Cai, W., Zhang, C., Suen, H. P., Ai, S., Bai, Y., Bao, J., et al. (2021). The 2020 China report of the Lancet Countdown on health and climate change. *The Lancet Public Health*, *6*(1), e64–e81. https://doi.org/10.1016/s2468-2667(20)30256-5

Chen, K., Huang, L., Zhou, L., Ma, Z., Bi, J., & Li, T. (2015). Spatial analysis of the effect of the 2010 heat wave on stroke mortality in Nanjing, China. *Scientific Reports*, *5*(1), 10816. https://doi.org/10.1038/srep10816

Chen, Y., & Li, Y. (2017). An inter-comparison of three heat wave types in China during 1961–2010: Observed basic features and linear trends. *Scientific Reports*, *7*, 45619. https://doi.org/10.1038/srep45619

Colwell, R. K., & Lees, D. C. (2000). The mid-domain effect: Geometric constraints on the geography of species richness. *Trends in Ecology & Evolution*, *15*(2), 70–76. https://doi.org/10.1016/s0169-5347(99)01767-x

Ding, T., Qian, W., & Yan, Z. (2010). Changes in hot days and heat waves in China during 1961–2007. *International Journal of Climatology*, *30*(10), 1452–1462. https://doi.org/10.1002/joc.1989

Dong, S., Xu, Y., Zhou, B., & Shi, Y. (2015). Assessment of indices of temperature extremes simulated by multiple CMIP5 models over China. *Advances in Atmospheric Sciences*, *32*(8), 1077–1091. https://doi.org/10.1007/s00376-015-4152-5

García-León, D., Casanueva, A., Standardi, G., Burgstall, A., Flouris, A. D., & Nybo, L. (2021). Current and projected regional economic impacts of heatwaves in Europe. *Nature Communications*, *12*(1), 5807. https://doi.org/10.1038/s41467-021-26050-z

Ge, J., Qiu, B., Wu, R., Cao, Y., Zhou, W., Guo, W., & Tang, J. (2021). Does dynamic downscaling modify the projected impacts of stabilized 1.5°C and 2°C warming on hot extremes over China? *Geophysical Research Letters*, *48*(6), e2021GL092792. https://doi.org/10.1029/2021gl092792

Gu, S., Huang, C., Bai, L., Chu, C., & Liu, Q. (2015). Heat-related illness in China, summer of 2013. *International Journal of Biometeorology*, *60*(1), 131–137. https://doi.org/10.1007/s00484-015-1011-0

Guo, H., Bao, A., Ndayisaba, F., Liu, T., Jiapaer, G., El-Tantawi, A. M., & De Maeyer, P. (2018). Space-time characterization of drought events and their impacts on vegetation in Central Asia. *Journal of Hydrology*, *564*, 1165–1178. https://doi.org/10.1016/j.jhydrol.2018.07.081

Hamed, K. H., & Rao, A. R. (1998). A modified Mann-Kendall trend test for autocorrelated data. *Journal of Hydrology*, *204*(1–4), 182–196. https://doi.org/10.1016/s0022-1694(97)00125-x

Keellings, D., & Moradkhani, H. (2020). Spatiotemporal evolution of heat wave severity and coverage across the United States. *Geophysical Research Letters*, *47*(9), e2020GL087097. https://doi.org/10.1029/2020gl087097

Li, D., Zhou, T., Zou, L., Zhang, W., & Zhang, L. (2018). Extreme high-temperature events over East Asia in 1.5°C and 2°C warmer futures: Analysis of NCAR CESM low-warming experiments. *Geophysical Research Letters*, *45*(3), 1541–1550. https://doi.org/10.1002/2017gl076753

Li, T. (2006). Origin of the summertime synoptic-scale wave train in the Western north Pacific. *Journal of the Atmospheric Sciences*, *63*(3), 1093–1102. https://doi.org/10.1175/jas3676.1

Liao, W., Liu, X., Li, D., Luo, M., Wang, D., Wang, S., et al. (2018). Stronger contributions of urbanization to heat wave trends in wet climates. *Geophysical Research Letters*, *45*(20), 11310–11317. https://doi.org/10.1029/2018gl079679

Lloyd-Hughes, B. (2012). A spatio-temporal structure-based approach to drought characterisation. *International Journal of Climatology*, *32*(3), 406–418. https://doi.org/10.1002/joc.2280

Lu, R.-Y., & Chen, R.-D. (2016). A review of recent studies on extreme heat in China. *Atmospheric and Oceanic Science Letters*, *9*(2), 114–121. https://doi.org/10.1080/16742834.2016.1133071

Luo, M., & Lau, N.-C. (2017). Heat waves in southern China: Synoptic behavior, long-term change, and urbanization effects. *Journal of Climate*, *30*(2), 703–720. https://doi.org/10.1175/jcli-d-16-0269.1

Luo, M., & Lau, N.-C. (2021). Increasing human-perceived heat stress risks exacerbated by urbanization in China: A comparative study based on multiple metrics. *Earth's Future*, *9*(7), e2020EF001848. https://doi.org/10.1029/2020ef001848

Luo, M., Ning, G., Xu, F., Wang, S., Liu, Z., & Yang, Y. (2020). Observed heatwave changes in arid northwest China: Physical mechanism and long-term trend. *Atmospheric Research*, *242*, 105009. https://doi.org/10.1016/j.atmosres.2020.105009

Lyon, B., Barnston, A. G., Coffel, E., & Horton, R. M. (2019). Projected increase in the spatial extent of contiguous US summer heat waves and associated attributes. *Environmental Research Letters*, *14*(11), 114029. https://doi.org/10.1088/1748-9326/ab4b41

Mondal, S., & Mishra, A. K. (2021). Complex networks reveal heatwave patterns and propagations over the USA. *Geophysical Research Letters*, *48*(2), e2020GL090411. https://doi.org/10.1029/2020gl090411

Mukherjee, S., & Mishra, A. K. (2021). Increase in compound drought and heatwaves in a warming world. *Geophysical Research Letters*, *48*(1), e2020GL090617. https://doi.org/10.1029/2020gl090617

Ning, G., Luo, M., Zhang, Q., Wang, S., Liu, Z., Yang, Y., et al. (2021). Understanding the mechanisms of summer extreme precipitation events in Xinjiang of arid Northwest China. *Journal of Geophysical Research: Atmospheres*, *126*(15), e2020JD034111. https://doi.org/10.1029/2020jd034111

O'Reilly, C., Larson, E., Richards, J. E., & Elsabbagh, M. (2021). Structural templates for imaging EEG cortical sources in infants. *NeuroImage*, *227*, 117682. https://doi.org/10.1016/j.neuroimage.2020.117682

Park, J., Choi, W., Tiesmeyer, S., Long, B., Borm, L. E., Garren, E., et al. (2021). Cell segmentation-free inference of cell types from in situ transcriptomics data. *Nature Communications*, *12*(1), 3545. https://doi.org/10.1038/s41467-021-23807-4

Perkins, S. E., & Alexander, L. V. (2013). On the measurement of heat waves. *Journal of Climate*, *26*(13), 4500–4517. https://doi.org/10.1175/jcli-d-12-00383.1

Perkins-Kirkpatrick, S. E., & Lewis, S. C. (2020). Increasing trends in regional heatwaves. *Nature Communications*, *11*(1), 3357. https://doi.org/10.1038/s41467-020-16970-7

Pfahl, S., & Wernli, H. (2012). Quantifying the relevance of atmospheric blocking for co-located temperature extremes in the Northern Hemisphere on (sub-) daily time scales. *Geophysical Research Letters*, *39*(12), L12807. https://doi.org/10.1029/2012gl052261

Reddy, P. J., Perkins-Kirkpatrick, S. E., & Sharples, J. J. (2021). Interactive influence of ENSO and IOD on contiguous heatwaves in Australia. *Environmental Research Letters*, *16*, 014004. https://doi.org/10.1088/1748-9326/ac3e9a

Ren, G., & Zhou, Y. (2014). Urbanization effect on trends of extreme temperature indices of national stations over mainland China, 1961–2008. *Journal of Climate*, *27*(6), 2340–2360. https://doi.org/10.1175/jcli-d-13-00393.1

Rosenfeld, A., & Pfaltz, J. L. (1966). Sequential operations in digital picture processing. *Journal of the ACM*, *13*(4), 471–494. https://doi.org/10.1145/321356.321357

Saeed, S., Van Lipzig, N., Müller, W. A., Saeed, F., & Zanchettin, D. (2014). Influence of the circumglobal wave-train on European summer precipitation. *Climate Dynamics*, *43*, 503–515. https://doi.org/10.1007/s00382-013-1871-0

Sharma, S., & Mujumdar, P. (2017). Increasing frequency and spatial extent of concurrent meteorological droughts and heatwaves in India. *Scientific Reports*, *7*(1), 15582. https://doi.org/10.1038/s41598-017-15896-3

Silversmith, W. (2021). *CC3d: Connected components on multilabel 3D images*. Retrieved from https://pypi.org/project/connected-components-3d/

Sun, Y., Zhang, X., Ren, G., Zwiers, F. W., & Hu, T. (2016). Contribution of urbanization to warming in China. *Nature Climate Change*, *6*, 706–709. https://doi.org/10.1038/nclimate2956

Wang, J., Chen, Y., Liao, W., He, G., Tett, S. F., Yan, Z., et al. (2021). Anthropogenic emissions and urbanization increase risk of compound hot extremes in cities. *Nature Climate Change*, *11*, 1084–1089. https://doi.org/10.1038/s41558-021-01196-2

Wang, J., Yan, Z., Quan, X.-W., & Feng, J. (2017). Urban warming in the 2013 summer heat wave in eastern China. *Climate Dynamics*, *48*(9–10), 3015–3033. https://doi.org/10.1007/s00382-016-3248-7

Watts, N., Amann, M., Arnell, N., Ayeb-Karlsson, S., Beagley, J., Belesova, K., et al. (2021). The 2020 report of the lancet countdown on health and climate change: Responding to converging crises. *The Lancet*, *397*(10269), 129–170. https://doi.org/10.1016/s0140-6736(20)32290-x

Wu, J., & Gao, X. (2013). A gridded daily observation dataset over China region and comparison with the other datasets. *Chinese Journal of Geophysics*, *56*(4), 1102–1111.

Wu, K., Otoo, E., & Suzuki, K. (2005). *Two strategies to speed up connected component labelingalgorithms*. No. LBNL-59102. Ernest Orlando Lawrence Berkeley NationalLaboratory.

You, Q., Jiang, Z., Kong, L., Wu, Z., Bao, Y., Kang, S., & Pepin, N. (2017). A comparison of heat wave climatologies and trends in China based on multiple definitions. *Climate Dynamics*, *48*(11–12), 3975–3989. https://doi.org/10.1007/s00382-016-3315-0

Zhao, W., Jiang, D., Peña Queralta, J., & Westerlund, T. (2020). MSS U-net: 3D segmentation of kidneys and tumors from CT images with a multi-scale supervised U-net. *Informatics in Medicine Unlocked*, *19*, 100357. https://doi.org/10.1016/j.imu.2020.100357